Determination of onset of bubbling and slugging in a fluidized bed using a dual-plane electrical capacitance tomography system

CrossMark

Cornelius Emeka Agu *, Lars-André Tokheim, Marianne Eikeland, Britt M.E. Moldestad

Department of Process, Energy and Environmental Technology, University College of Southeast Norway, 3918 Porsgrunn, Norway

HIGHLIGHTS

- Fluidization index decreases with an increasing Archimedes number.
- The bed height for stable slug flow depends on the particle size distributions.
- Both the particle size and the bed height influence the transition from bubbling to slugging.
- The dependency of slug index on the bed height decreases with an increasing Archimedes number.

ARTICLE INFO

ABSTRACT

For a successful application of fluidized beds in chemical reactions and solids circulation, the boundary of regime of operation such as bubbling and slugging regimes, needs to be clearly defined. This study provides a method for determining the onset of fluidized bed regimes using a two-plane electrical capacitance tomography (ECT) sensor. The method involves computation and analysis of standard deviations of the solids fraction recorded at each plane of the ECT sensor for different superficial gas velocities. The experimental study is based on two different samples of 100–550 μm glass particles and one sample of 150–450 μm limestone particles. The results show that the onset of bubbling is determined when a bubble is first observed in the upper plane. The onset of slugging is obtained at the peak of the difference in the solids fraction fluctuation between the two planes, which is determined at the point where the rates of increase in the fluctuations are the same in both planes. The method developed in this study provides a means of obtaining accurate superficial gas velocities at the onset of slugging in fluidized beds.

© 2017 The Authors. Published by Elsevier B.V. This is an open access article under the CC BY-NC-ND license (http://creativecommons.org/licenses/by-nc-nd/4.0/).

1. Introduction

1.1. Background

Application of fluidized beds in processes involving chemical reactions and solids circulation, for example catalyst regeneration or heat transfer, requires a well-defined and stable contact regime [1]. Maintaining the appropriate regime is a major challenge in optimizing the design of fluidized bed reactors due to limited understanding of the dynamics characteristics of fluidized beds [2]. The properties describing the dynamic behaviour of a fluidized bed include the variation of bubble shape, bubble size and solids fraction distribution at different regimes [3].

When a bed is fluidized, it may transit from one flow regime to another depending on the gas velocity. The fluidized bed regimes include bubbling, slugging, turbulent fluidization, fast fluidization and pneumatic conveying regimes [4]. The transition from one regime to another is characterized with a certain superficial gas velocity and a certain bed void fraction. Being able to determine when transition occurs is important for the design of fluidized bed reactors. The most common method to determine the minimum fluidization velocity is by taking measurement of pressure drop in the bed at different superficial gas velocities. The onset of fluidization corresponds to the point where the pressure drop across the bed reaches a maximum value. The minimum fluidization velocity may vary with temperature, pressure or both depending on the properties of the bed [4].

The understanding of transition from the fluidized state to the bubble regime is not as good as that of minimum fluidization [5]. In a bed of larger particles, for example 100–1000 μm, many researchers have observed that bubbles appear as soon as the

bed is fluidized. For fine particles such as fluid catalyst cracking particles, the bed expands significantly after the minimum fluidization before bubbles appear. This means that the superficial gas velocity at which bubbling occurs is higher than the minimum fluidization velocity. The difference between the minimum bubbling velocity and the minimum fluidization velocity is attributed to the significant magnitude of inter-particle forces between the fine particles [5].

With further increase in the gas velocity, the bubbles grow in size, and when the bubble size is in the order of the bed diameter, the bed slugs [6–8]. The superficial gas velocity at which a slug appears in the bed is the onset of slugging. The occurrence of slugs depends on the bed aspect ratio defined as the ratio of bed height to bed diameter, and on the particle size. In a large diameter bed, slugs rarely occur because the bubbles will not be able to grow in size up to the bed diameter. When a bed contains fine particles, it will be difficult for it to slug. This is because the stable bubble size in the bed is lower than the bed diameter due to competitive bubble coalescence and bubble splitting [4,5]. Slugs can be in the form of round-nosed structure in beds of materials that can be fluidized easily, or in form of square-nosed structure in difficult-to-fluidize bed materials [9].

The transition between regimes in fluidized beds is accompanied by the solids fraction fluctuation, pressure fluctuation and bed expansion [5]. Different techniques used in fluidized bed studies measure these properties directly or indirectly. Such measurement techniques include pressure transducers, capacitance probes, optical fibre probes, etc. Since different techniques may provide different information about the bed [10], a systematic analysis is required to evaluate the information from the different measurement methods [11]. Among other statistical tools, standard deviation is widely used in analysing the measurement data. The standard deviation can be used to measure the fluctuation of dynamic behaviour of a fluidized bed. In this paper, the fluctuation of the solids fraction is used to determine the behaviour of the fluidized beds. The solids fraction is measured using electrical capacitance tomography (ECT). ECT is a non-intrusive sensor used to measure the relative permittivity between two non-conducting phases. It is non-intrusive as it does not interrupt the flow or bed it measures. In addition to being relatively cheap, fast and flexible to use, ECT can be used in real-time applications, and this makes it more versatile compared to other tomographic methods such as X-ray, γ-ray and ultrasonic tomography [2]. Despite its numerous advantages, the temperature and size of the bed limit its application. In a bed with diameter larger than 30 cm, ECT is not reliable due to the nature of the soft field on which the measurement principle depends [12].

1.2. Previous works

Several studies have been published on different fluidized bed regimes and their transitions. Different techniques employed in identifying a fluidized bed regime are visual detection and analyses of bed property signals such as pressure fluctuation, voidage fluctuation and bed expansion. In a bubbling fluidized bed, the fluctuations arise due to propagation of pressure waves generated during bubble formation, bubble movement, bubble coalescence/splitting and bubble eruption at the surface of the bed [5]. These fluctuations are often analysed in terms of standard deviation, power spectra distribution and probability density function obtained over the measurement period.

The onset of transition from fixed bed to particulate regime (non-bubbling fluidized state) has been widely obtained from the measurement of pressure drops or their fluctuations at different gas velocities [4]. This method has been found to give consistent results independent on the particle size, bed diameter and bed sta-

tic height. The minimum fluidization velocities have also been obtained from analyses of absolute pressure fluctuation [13–15], and void or solids fraction fluctuation for larger particles [16,17] on the assumption that the minimum fluidization condition coincides with that of bubbling regime.

The transition into bubbling regime is usually visualized as the gas velocity where the first bubble is seen erupting from the bed surface [18]. On the assumption that the fluctuations in fluidized beds are due to bubble formation and passages, different researchers have obtained the onset of bubbling regime at the gas velocity where the pressure [19] or solids fraction [17] fluctuations begins to rise from zero. Leu and Tsai [19] also observed that the minimum bubbling velocity is independent on the bed static height but on the location of the sensors for measurement of the absolute pressure fluctuations.

Slugging fluidized beds have been widely studied due to inconsistencies in the results presented by several authors. Different factors may be responsible for this variation, and these include sensor position during the measurement, variation in the bed diameter, bed height, particle size and particle shape [20]. Broadhurst and Becker [21] used visual detection to identify slugs, where the onset of slugging regime was obtained as the minimum gas velocity at which a bubble is seen to have a continuous floor around the bed circumference before arriving the surface of the bed. This method was shown to produce successful results where the bed height is above twice the bed diameter. Ho et al. [22] measured the minimum slugging velocity at a point where the absolute bubble rise velocity is locally minimum near the transition zone. The bubble rise velocity was obtained from the cross correlation of two different pressure fluctuation signals measured in the bed. In different beds of glass and sand particles, 358 – 1112 μm, Ho et al. found that the minimum slugging velocity is independent on the bed diameter and bed height.

Dimattia et al. [20] used the same technique as Baeyens and Geldart [7] to predict the onset of slugging regime. Baeyens and Geldart [7] identified the flow of slugs in a fluidized bed as either a single slug or a complete slugging. A single slug is observed when the pressure fluctuation spike passes through the datum established at the minimum fluidization condition while complete slugging is obtained when the slug frequency is constant for any change in the gas velocity. For larger particles (diameter above 500 μm), Dimattia et al. [20] observed that the minimum slugging velocity is independent on the bed height due to low resistance to gas flow offered by these particles. In a similar technique, Kong et al. [18] identified a slug flow when a negative amplitude followed by a positive amplitude of the pressure fluctuation crosses a datum line. In their results, Kong et al. concluded that the minimum slugging velocity for fine particles (diameter below 100 μm), is independent on the initial bed height.

Noordergraaf et al. [23] distinguished slugging from bubbling regime by the occurrence of single predominant frequency and a more regular pressure fluctuation pattern. The predominant frequencies are due to passage of single chain of bubbles when the bubble diameter is more than half of the bed diameter. In large particle systems, Noordergraaf et al. obtained the minimum slugging velocity at the point where the curve of predominant frequency versus gas velocity is minimum. For glass particles, 450–540 μm, no predominant frequency was found. The authors concluded that even for fine particles the method will not give results since the pressure fluctuations associated with their fluidization are too small to be sensed by the pressure transducers.

Du et al. [2] used ECT sensors to measure the solids fraction fluctuation at different gas velocities above the minimum bubbling velocity in different beds with diameters: 0.05, 0.1 and 0.3 m and initial bed height 0.5 m. The authors obtained the minimum slugging velocity at the peak of the solids fraction fluctuation. For the

FCC particles, 60 μm, the authors showed that the fluidized bed passes through slugging to the turbulent regime only in the 0.05 m bed. In the larger bed diameters, the system moved from bubbling to turbulent regime, where the onset of turbulent fluidization was obtained at the peak of the solids fraction fluctuation. These results are not in agreement with Baeyens and Geldart [7] observations. Baeyens and Geldart [7] correlated data from different beds: mean particle size ranging from 55 to 3380 μm, particle density in the range of 850 to 2800 and bed diameter in the range of 0.05 to 0.3 m. Their correlation have been widely used for predicting the minimum slugging velocity for different particle properties, bed heights and diameters.

In the bed of 216 μm glass particles (bed height to diameter ratio of 9.8), Bi [5] measured the voidage fluctuation using optical fibre probes. The experiment was conducted to illustrate the transition to turbulent fluidization through slugging regime. Bi [5] noted that the minimum velocity at transition to turbulent flow is obtained at the peak of the voidage fluctuation. Although there is a gradual drop in their results before the peak, the boundary between the bubbling and slugging zones is not clearly marked.

Considering the discrepancies among the results from different literatures, the study of regime transition in fluidized beds is still an ongoing process. In this paper, the method of using information from both planes of a two-plane ECT system for determining the onset of fluidized bed regimes is applied. Finding the actual point at the onset of every regime is vital for a successful fluidized bed application. In systems where the transition is gradual, it may be difficult to determine the exact velocity and void fraction at the onset of the regime. The aim of this paper is to exploit a possible way to combine the information from both planes of the ECT sensor to determine the exact velocities at the onset of slugging.

The study is carried out applying a cold fluidized bed rig using different particle size distributions, bed materials and bed heights. The statistical analysis is based on the standard deviation of the solids fraction, and all the computations are done in MATLAB. The minimum fluidization velocities of the particles used in this study are first obtained from the pressure drop measurement across the bed. This set of values is used to validate the measurements from the ECT sensors. The superficial gas velocities obtained at the onset of fluidization, bubbling and slugging are compared with the values calculated based on the empirical expressions for the respective regimes.

In the remaining parts of this paper, the empirical correlations for prediction of the onset of regime transition in a fluidized bed are presented first, then a description of the experimental setup is given, and finally the results are presented and discussed.

2. Minimum superficial gas velocities at fluidization, bubbling and slugging

In this study, the velocity at the onset of fluidization, referred to as the minimum fluidization velocity is denoted by U_{mf} [m/s]. U_{mf} is obtained by balancing the net weight of the bed with the drag force between the fluid and the particles in the bed.

$$(1 - \varepsilon_{mf})(\rho_s - \rho_g)g = \frac{\beta_d U_{mf}}{\varepsilon_{mf}^2} \tag{1}$$

Here, ε_{mf} is the void fraction at minimum fluidization [-], ρ_s is the particle density [kg/m^3], ρ_g is the fluid density [kg/m^3] and g [m/s^2] is the acceleration due to gravity. β_d [kg/(m^3 s)] is the momentum transfer coefficient between the two phases. The accuracy of the U_{mf} calculation depends on the drag model used. A number of drag models have been published in the literature

[24–26]. The simpler and more common one is that given by Gidaspow [27]. It was derived from Ergun's equation of pressure drop in fixed beds and is shown in Eq. (2).

$$\beta_d = 150 \frac{(1 - \varepsilon_{mf})^2 \mu_g}{\varepsilon_{mf} (\varphi_s d_s)^2} + 1.75 \frac{\rho_g U_{mf}(1 - \varepsilon_{mf})}{\varepsilon_{mf} \varphi_s d_s} \tag{2}$$

Here, μ_g is the fluid dynamic viscosity [Pa.s], d_s the average diameter of the particles [m] and φ_s the particle sphericity [-]. According to Ergun [28], the pressure drop in a fixed bed can be obtained from

$$\frac{\Delta P}{\Delta L} = 150 \frac{\varepsilon_{s0}^2}{(1 - \varepsilon_{s0})^3} \frac{\mu_g U_0}{(\varphi_s d_s)^2} + 1.75 \frac{\varepsilon_{s0}}{(1 - \varepsilon_{s0})^3} \frac{\rho_g U_0^2}{\varphi_s d_s} \tag{3}$$

where $\frac{\Delta P}{\Delta L}$ is the pressured drop per unit length across the bed [Pa/m] and ε_{s0} is the volume fraction of the solid particles in a fixed state [-]. Ergun's model is developed for a dense phase system where the solids concentration is greater than 0.2. The drag model based on the correlation of Gibilaro et al. [29] can be used for the entire range of solids fraction, and may be described as

$$\beta_d = C_d \frac{\varepsilon_{mf}(1 - \varepsilon_{mf})}{\varphi_s d_s} \rho_g U_{mf} \varepsilon_{mf}^{-1.80} \tag{4}$$

where C_d is the single particle drag coefficient [-], given by

$$C_d = 0.336 + \frac{17.3}{Re_{s,mf}} \tag{5}$$

Here, $Re_{s,mf}$ is the modified particle Reynolds number [-] at minimum fluidization conditions, expressed as

$$Re_{s,mf} = \frac{(1 - \varepsilon_{mf})}{\varepsilon_{mf}} \frac{\rho_g U_{mf} \varphi_s d_s}{\mu_g} \tag{6}$$

In addition to the momentum transfer coefficient, the void fraction at minimum fluidization is another parameter that determines the accuracy of the U_{mf} calculation. Similar to U_{mf}, ε_{mf} is a bed property, thus its accurate measurement or evaluation is important. ε_{mf} has been observed to strongly depend on the particle sphericity, and according to Wen and Yu [30] its approximate value can be obtained through Eqs. (7) or (8), depending on the particle Reynolds number at minimum fluidization conditions.

$$\varepsilon_{mf}^3 = 0.091 \frac{(1 - \varepsilon_{mf})}{\varphi_s^2}; \ Re_{mf} < 20 \tag{7}$$

$$\varepsilon_{mf} = \left(\frac{0.071}{\varphi_s} \right)^{1/3}; \ Re_{mf} > 20 \tag{8}$$

The onset of bubbling depends on the particle size. For larger particles, the minimum superficial gas velocity U_{mb} in the bubble regime is about the same as the minimum fluidization velocity [31]. However, with fine particles, Geldart and Abrahamsen [32] found that U_{mb} strongly depends on the fraction of particles smaller than 45 μm that are present in the bed. The ratio $\frac{U_{mb}}{U_{mf}}$ for these types of particles may be expressed as

$$\frac{U_{mb}}{U_{mf}} = \frac{2300 \rho_g^{0.13} \mu^{0.52}}{d_s^{0.8} (\rho_s - \rho_g)^{0.93}} \exp(0.72 w_{45}), \tag{9}$$

where w_{45} is the weight fraction of particles smaller than 45 μm [-].
Geldart and Abrahamsen [32] also correlated the void fraction at minimum bubbling condition [33] as given by

$$\frac{1 - \varepsilon_{mb}}{1 - \varepsilon_{mf}} = \left(\frac{U_{mb}}{U_{mf}} \right)^{0.22} \tag{10}$$

where ε_{mb} is the average void fraction of the bed at minimum bubbling condition.

The transition from bubbling to slugging strongly depends on the bed aspect ratio h_0/D_b, where h_0 is the bed height [m] in a fixed state, and D_b is the bed diameter [m]. Yang [34] showed that in addition to ensuring sufficiently high superficial gas velocity, slugging will occur if $h_0/D_b \geqslant 2$. According to Geldart [35], the superficial gas velocity U_{ms} at the onset of slugging can be obtained from

$$U_{ms} = U_{mf} + 0.0016(60D_b^{0.175} - h_{mf})^2 + 0.07(gD_b)^{0.5} \qquad (11)$$

where all the length units are in centimetres, and h_{mf} is the bed height at minimum fluidization conditions.

When the bed contains particles of different sizes, the mean particle diameter used in Eqs. (1)–(11) is obtained as given in Eq. (12), which ensures that the total surface area of the particles for the same total bed volume remains the same [4].

$$d_s = \frac{1}{\sum \left(\frac{w_s}{d_s}\right)_i} \qquad (12)$$

Here, d_{si} is the diameter of the individual particle having a weight fraction w_{si} in the bed.

3. Experimental

3.1. Experimental setup

The setup used in this work consists of a cylindrical column of diameter 10.4 cm and height 1.4 m. The bottom of the column is fitted with a porous plate and an air supply hose. The porous plate ensures even distribution of air in the bed. The measuring equipment is a dual-plane ECT sensor. The system is shown in Fig. 1. The sensors are located at two different positions, 15.7 cm and 28.7 cm above the distributor. Each sensor consists of 12 electrodes, uniformly distributed around the plane circumference. The cross-section of each sensor is divided into 32×32 square pixels, of which 812 pixels lie within the bed as shown in Fig. 1b. Each pixel holds a normalized relative permittivity between 0 and 1. When the sensors are energized by the applied voltage, the capacitance between each pair of electrodes is measured and converted into permittivity values according to the relationship $C = SP$ [36]. Here, C is an $M \times 1$ capacitance matrix with $M = 66$ (number of inter-electrode pairs), P is an $N \times 1$ relative permittivity matrix with $N = 1024$ (number of pixels) and S is an $M \times N$ sensor sensitivity matrix. The relative permittivity is evaluated based on the Linear Back Projection algorithm [36].

The experiments were performed with limestone and glass particles using compressed air at ambient temperature. These materials were chosen because the difference in their properties gives different behaviour in the fluidized beds. The glass particles may exhibit smooth fluidization, as they are close to spherical in shape and are not adhesive in nature. On the contrary, limestone particles are adhesive and irregular in shape, which may influence fluidization behaviour negatively. In spite of this, limestone may be a good bed material for chemical synthesis due to its catalytic property and ability to withstand high temperature. Using glass particles of different size distributions will also help to investigate the influence of particle size distribution on the fluidized bed regime transition. For each set of particles, the experiments were conducted with three different bed heights: 52, 58 and 64 cm.

Table 1 shows the properties of the bed materials and the range of superficial air velocities used in the experiment. In the experiments, the ECT sensors were first calibrated for the lower permittivity when the column was empty, and then for the higher permittivity value by filling up with the appropriate particles to a height between 50.0 and 64.0 cm which ensured that the upper plane was well covered with the particles. The lower and higher
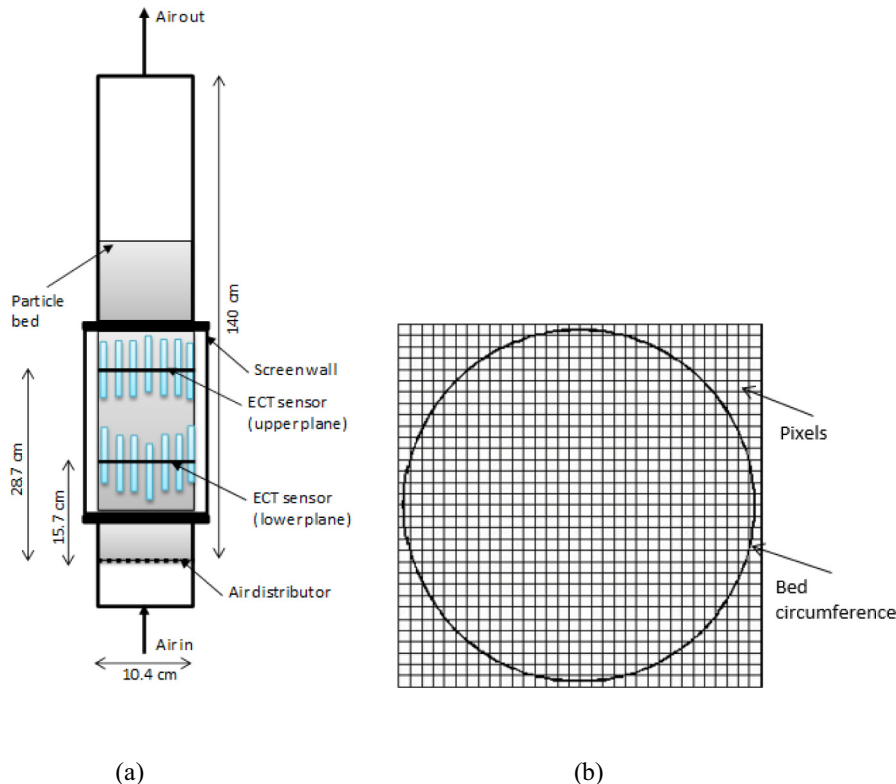

(a)   (b)

Fig. 1. (a) Schematic illustration of a cold fluidized bed where two plane ECT sensors are used to measure solids fraction. (b) Cross-section of the bed divided into 812 pixels.

Table 1
Bed properties with the associated range of superficial air velocity.

Materials	Material density [kg/m^3]	Particle size [μm]	Mean particle diameter [μm]	Solids fraction in fixed state [-]	Sphericity [-]	Superficial air velocity [m/s]
Glass	2500	100–550	261	0.62	0.96	0.039–0.334
Glass	2500	100–550	188	0.63	0.96	0.010–0.275
Lime stone	2837	150–450	293	0.51	0.84	0.039–0.373

permittivity values defining the range of the measurement are normalized into values 0 and 1, respectively. The normalized relative permittivity ε_r [-] is a measure of volume fraction of solids in the bed. The volume fraction of particles ε_s [-] at any point in the plane is obtained from $\varepsilon_s = \varepsilon_{s0}\varepsilon_r$. The observed value of the fixed bed solids fraction ε_{s0} is given in Table 1.

After the sensor calibration, the air supply line was opened and the superficial air velocity was gradually increased until the full range was covered. For each air velocity, the images of solids distribution at each plane of the ECT sensors were recorded for 60 s. The image data were captured at a frame frequency of 100 Hz, giving 6000 frames over the 60 s. The recorded image data were exported for analysis in MATLAB. To reduce the experimental random error, five different measurements were taken at interval of 2 min for each air velocity. These five data sets were analysed separately, and their average was taken.

3.2. Measurement of solids fraction fluctuation

At a given gas velocity, the solids fraction fluctuation is measured by computing the standard deviation of the plane-average solids fraction over the measurement periods. For each pixel in a given plane, the solids fraction is measured with the ECT sensor as described in 3.1, and then stored in a matrix **A**(i,j,k). The indices, "i" and "j" locate each pixel in a 32×32 plane; see Fig. 1b, while the index "k" is the time frame at which the pixel value is obtained. The plane-average solids fraction, ε_{sk} at a given frame is then obtained from

$$\varepsilon_{sk} = \frac{1}{n}\sum_{i}^{32}\sum_{j}^{32}A(i,j,k)$$

Over the entire frames, the time average solids fraction, ε_s at each plane is computed from

$$\varepsilon_s = \frac{1}{N}\sum_{k=1}^{N}\varepsilon_{sk}$$

The standard deviation σ_p of the solids fraction in each plane at a given gas velocity is then computed from

$$\sigma_p = \sqrt{\frac{1}{N-1}\sum_{k=1}^{N}(\varepsilon_{sk}-\varepsilon_s)^2}$$

Here, $n = 812$ is the number of pixels within each plane and $N = 6000$ is the number of frames taken. The subscript "p" denotes upper or lower plane.

4. Results and discussion

First, to determine the minimum fluidization velocity, pressure measurements for the beds of limestone and glass particles with mean size 261 μm were recorded in a separate cold fluidized bed fitted with pressure sensors; see [37] for detailed description of the experimental setup. The results are shown in Fig. 2. The
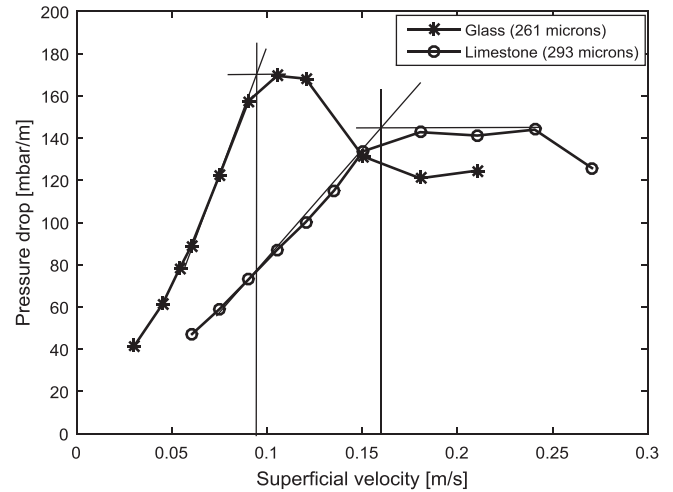

Fig. 2. Pressure drop as a function of the superficial air velocity in beds of lime stone particles (mean diameter 293 μm) and glass particles (mean diameter 261 μm), used to determine the particle minimum fluidization velocity.

minimum fluidization velocities of limestone and glass particles are 0.157 m/s and 0.095 m/s, respectively.

Fig. 3 shows the behaviour of the 261 μm glass particles over time at different velocities. The initial bed height was 64.0 cm. The results show that as the air velocity is increased the bed moved from the static state (Fig. 3a) through the bubble regime (Fig. 3b and c) to the slow-rising bubble (or slug) regime (Fig. 3d). Figs. 4 and 5 show that the 188 μm glass particles and limestone particles respectively have the same type of behaviour, but the transitions occur at different velocities. A bubble region in this work is regarded as where the solids fraction is 0.2 or less as indicated in the colorbars.

The superficial air velocity at the onset of each regime can be obtained by analysing the standard deviation of the solids fraction for the range of the superficial gas velocities used. Plots of the standard deviations against the superficial air velocities in both planes are shown in Fig. 6 for the 261 μm glass particles, Fig. 7 for the 188 μm glass particles and Fig. 8 for the limestone particles. The standard error bars are also shown in each of the plots to indicate how the solids fraction fluctuations measured in the five different measurements taken at each air velocity, spread around the mean value reported in this study. As the standard error for each data point is very small, the mean value of the solids fraction fluctuation used in the further analysis, is reliable. The difference in the upper and lower planes standard deviation ($\sigma_{upper} - \sigma_{lower}$) are also shown in the respective figures.

As shown in Figs. 6–8, the solids fraction fluctuations increase rapidly from 0 (zero) due to bubble passage and increase in bubble rise velocity as the gas velocity increases. With increasing gas velocity, the bubbles grow rapidly and increase in size, resulting in the increase in the solids fraction fluctuation. After a certain velocity, the rate of increase in the fluctuations decreases when the bubble approaches a stable size. This region of decreasing rate
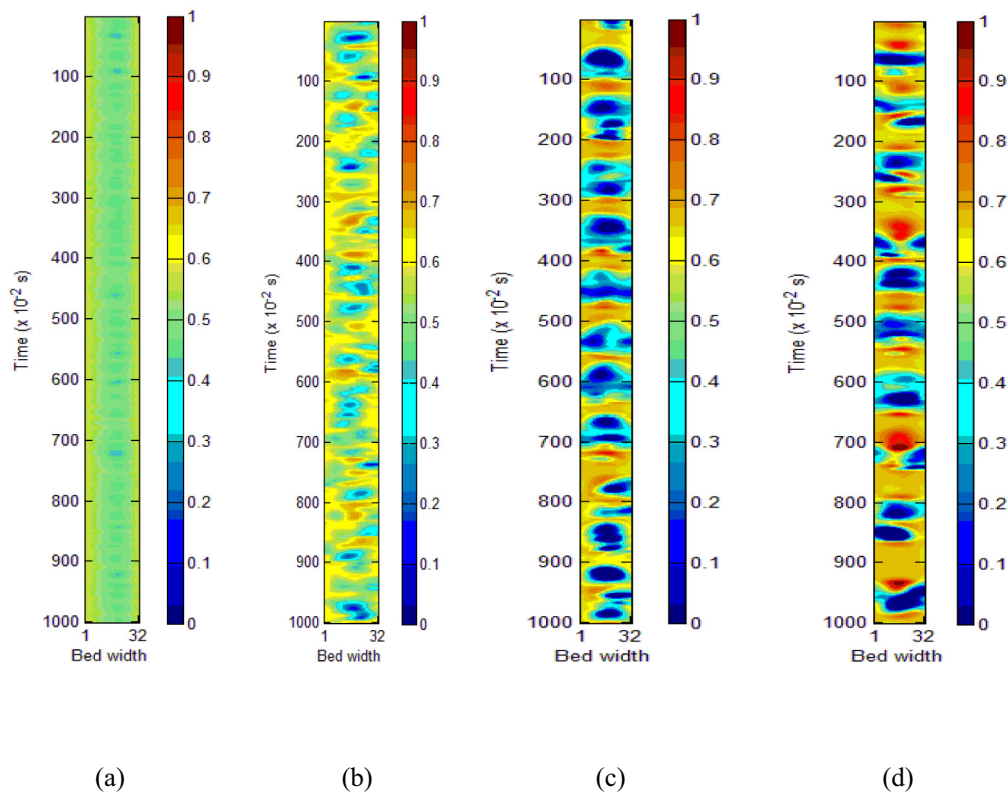
Fig. 3. Images from the upper plane ECT sensor stacked in time for the first – 10 s of the flow in a bed of glass particles (mean diameter 261 μm) at different superficial air velocities (a) 0.088 m/s, no sign of bubble in the plane. (b) 0.098 m/s, bubbles emerge in the plane. (c) 0.137 m/s, bubbles coalesce and become larger in the plane. (d) 0.157 m/s, the frequency of bubble rise decreases as the bubbles become even larger. Bed height is 64.0 cm; time axis increases from top to bottom.

of solids fraction fluctuation in the bed marks the slugging regime. In Fig. 6, for example, the solids fraction fluctuation begins to increase above zero at a velocity of about 0.088 m/s which corresponds to the onset of fluidization shown in Fig. 3a. As there is no sign of bubble in Fig. 3a, it means that the bed was not bubbling at the minimum fluidization velocity. The behaviour shown in Fig. 3 indicates that the velocity at onset of bubbling lies between 0.088 and 0.098 m/s. Similarly, Figs. 7 and 8 show that the beds of 188 μm glass and limestone particles begin to bubble when solids fraction fluctuation are significantly above zero in the upper plane. This shows that there could be factors other than bubble formation and passage responsible for the fluctuations in the fluidized bed. According to Bi [5], this may be due to self-excited oscillation of fluidized particles near the gas distributor.

As there is no clear demarcation between the particulate and bubbling regimes, it is difficult to obtain the minimum bubbling velocity from Figs. 6–8. The onset of bubbling in this study is obtained where a significant bubble is first observed in the upper plane, and these are virtually detected as shown in Figs. 3–5. With further increase in gas velocity, the solids fraction fluctuations in both planes increase. Within a certain range of gas velocity, the increase in the solids fraction fluctuation is almost linear in the upper plane and exponential in the lower plane. When the bubble reaches a stable size (such as that in the slugging) at a higher gas velocity, the rate of increase in the solids fraction fluctuation decreases and then remains constant with further increase in the gas velocity. This can be seen from Figs. 3 and 6. Because $\frac{h_0}{D_b} = 6.15$ (>2), the decrease in the rate of solids fraction fluctuation indicates a transition from bubbling to slugging. As the change in the rate of increase in the solids fraction fluctuation is gradual espe-

cially in the lower plane, it is difficult to determine the exact gas velocity at the onset of slugging from any of the planes.

The patterns of the curve of solids fraction fluctuation σ_{upper} in the upper plane and that σ_{lower} in the lower plane show that even when the rate of increase in σ_{upper} value decreases, the rate of increase in σ_{lower} value still increases. Considering the curve presenting the difference in the standard deviations ("Difference in fluctuation") in each of the Figs. 6, 7 and 8, it can be seen that this curve increases from zero as the gas velocity is raised above the minimum fluidization velocity. The difference in fluctuation $\sigma_{upper} - \sigma_{lower}$ measures the relative change in the rate of increase in the solids fraction fluctuations between the upper and lower planes. The $\sigma_{upper} - \sigma_{lower}$ curve peaks at a certain velocity, where the rate of increase in solids fraction fluctuation in the upper plane equals that in the lower plane. For velocities below the velocity at the peak, the rate of increase in the solids fraction fluctuation in the upper plane is higher than that in the lower plane, indicating that the bed is bubbling. Beyond the peak velocity, the rate of increase in the solids fraction fluctuation in the lower plane is higher than that in the upper plane, indicating that the bed is slugging. The gas velocity at the peak corresponds to the minimum slugging velocity. Because of the uncertainties in identifying the exact point the $\sigma_{upper} - \sigma_{lower}$ curve peaks, this method may be difficult to use in obtaining the onset of slugging velocity.

Fig. 9 shows the rates of increase in the solids fraction fluctuation obtained in both planes for the bed of 261 μm glass particles. The increase in the solids fraction fluctuation rate is obtained from the ratio $\frac{\Delta\sigma}{\Delta U_0}$ [s/m], where the operator Δ indicates a change and U_0 is the superficial gas velocity [m/s]. It can be seen that the $\frac{\Delta\sigma}{\Delta U_0}$ curve
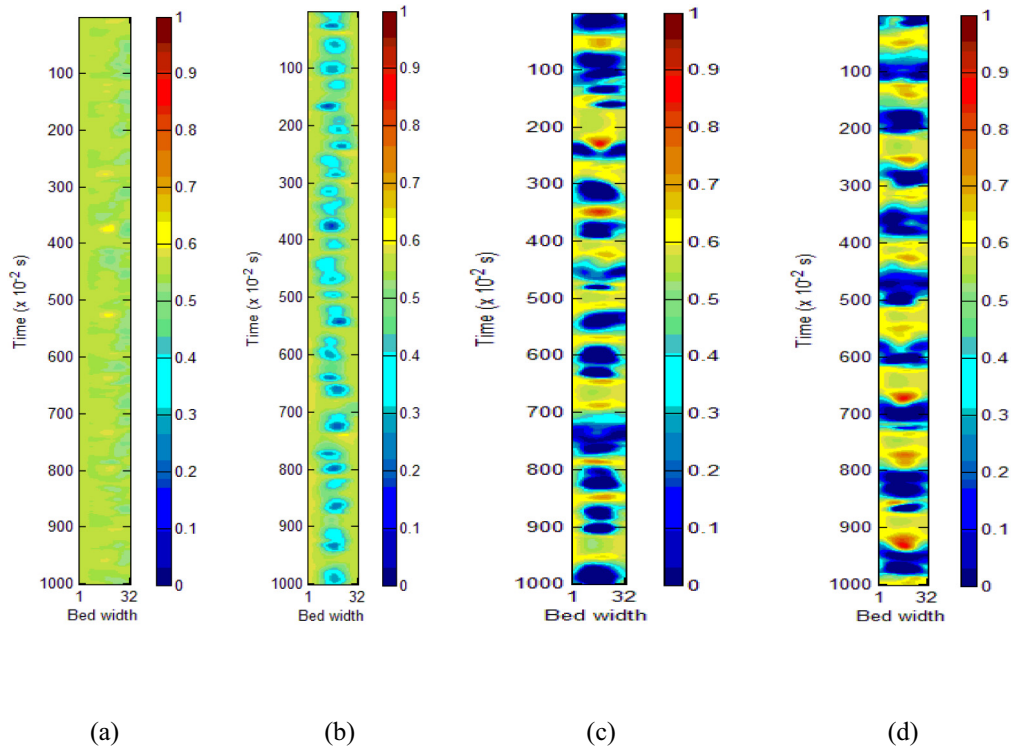
Fig. 4. Images from the upper plane ECT sensor stacked in time for the first – 10 s of the flow in a bed of glass particles (mean diameter 188 μm) at different superficial air velocities (a) 0.039 m/s, no sign of bubble in the plane. (b) 0.049 m/s, bubbles emerge in the plane. (c) 0.128 m/s, bubbles coalesce and become larger in the plane. (d) 0.157 m/s, slugs rise in the plane. Bed height is 52.0 cm; time axis increases from top to bottom.
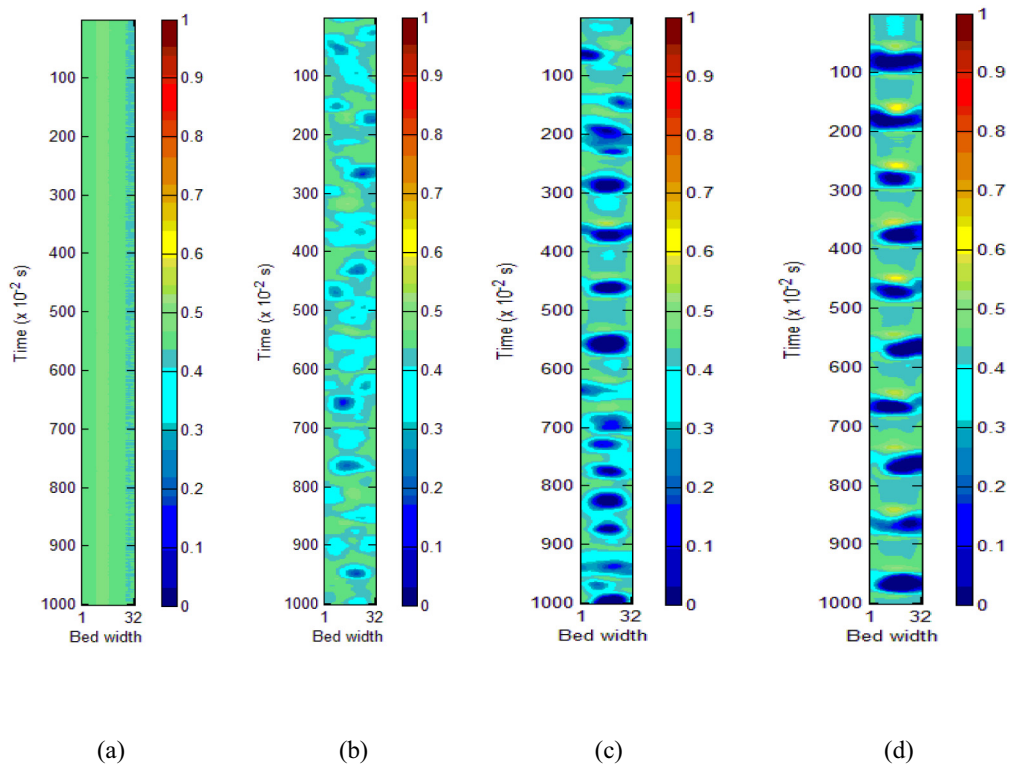

Fig. 5. Images from the upper plane ECT sensor stacked in time for the first – 10 s of the flow in a bed of limestone particles (mean diameter 293 μm) at different superficial air velocities (a) 0.137 m/s, no sign of bubble in the plane. (b) 0.157 m/s, bubbles emerge in the plane. (c) 0.216 m/s, bubbles coalesce and become larger in the plane. (d) 0.235 m/s, the frequency of bubble rise decreases as the bubbles become even larger. Bed height is 52.0 cm; time axis increases from top to bottom.
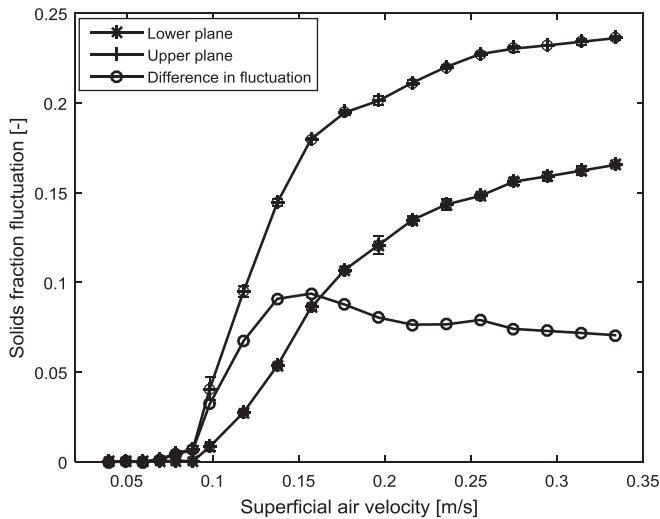
Fig. 6. Solids fraction fluctuation as a function of superficial air velocity in a bed of glass particles (mean diameter 261 μm), showing values for the upper plane, lower plane and their difference.
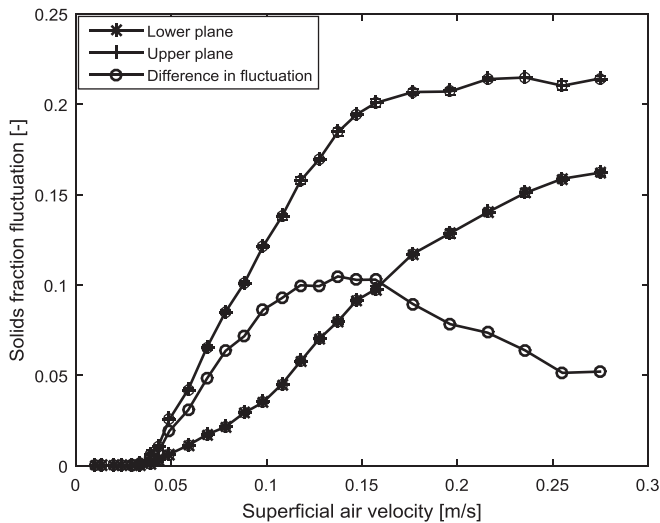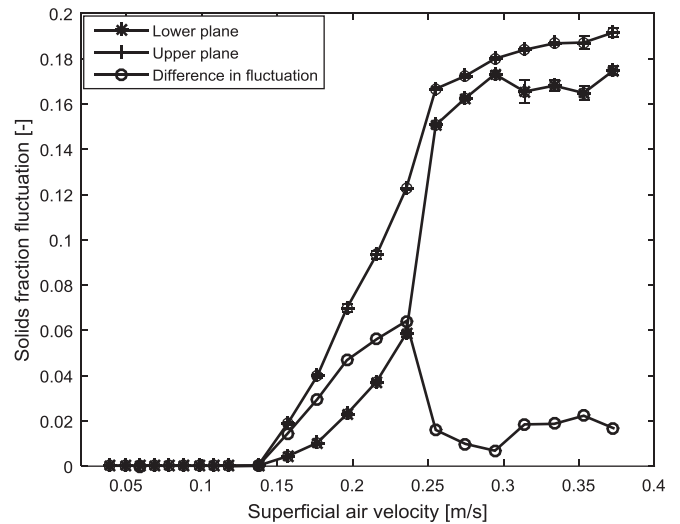

Fig. 8. Solids fraction fluctuation as a function of superficial air velocity in a bed of limestone particles (mean diameter 293 μm), showing values for the upper plane, lower plane and their difference.
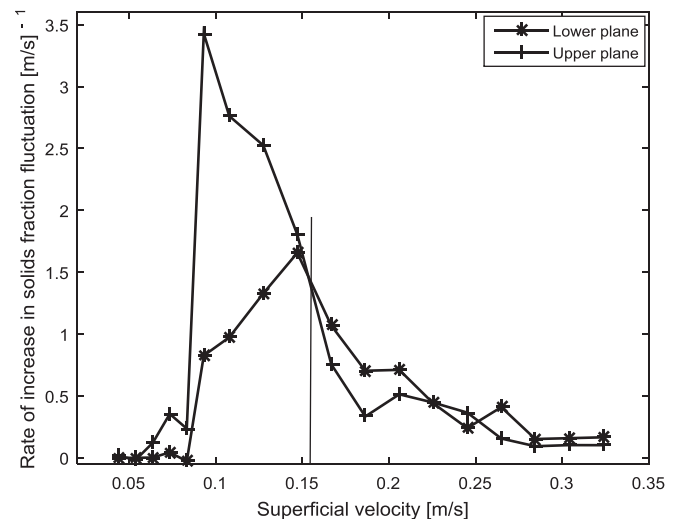

Fig. 7. Solids fraction fluctuation as a function of superficial air velocity in a bed of glass particles (mean diameter 188 μm), showing values for the upper plane, lower plane and their difference.

Fig. 9. Rate of solids fraction fluctuation increase as a function of superficial air velocity in a bed of glass particles (mean diameter 261 μm). The vertical line through the point of intersection of the two curves indicates the onset of slugging.

for the upper plane begins to decrease after a velocity of about 0.1 m/s while $\frac{\Delta\sigma}{\Delta U_0}$ curve for the lower plane is still increasing. This gas velocity is below the minimum slugging velocity, thus the bed will still be in bubbling zone. Beyond the point of intersection of both curves, the $\frac{\Delta\sigma}{\Delta U_0}$ values decrease in both planes towards a stable value. The decrease in $\frac{\Delta\sigma}{\Delta U_0}$ values in both planes indicates that the bed is slugging. Similar behaviour are also observed for all the particles studied in this work. The intersection of the $\frac{\Delta\sigma}{\Delta U_0}$ curves indicates the onset of slugging, which can be obtained at that point. This method for identifying the minimum slugging velocity depends on the values of velocity plotted against $\frac{\Delta\sigma}{\Delta U_0}$ values. If the lower value U_{01} in the change $\Delta U_0 = U_{02} - U_{01}$ is used, the corresponding minimum slugging velocity will be lower. A more accurate result is obtained when $\frac{\Delta\sigma}{\Delta U_0}$ is plotted against the average velocity $\frac{1}{2}(U_{02} + U_{01})$.

It should be noted that this approach of finding the onset of slugging is possible because of the sufficient gap between the two planes. As observed during the experiments, the upper part of the bed showed high bubbling activities and signs of slugging earlier than the lower part. This is probably because the location of the upper plane $\frac{L_u}{D_b} = 2.76$ is greater than 2 (precondition for slugging) while that of the lower plane $\frac{L_l}{D_b} = 1.51$ is less than 2.

In addition, the results show that the bed of the 261 μm glass particles and that of the 188 μm glass particles show similar flow behaviour. Transitions from fixed state to fluidized state and from bubbling to slugging as shown in Figs. 6 and 7 are smooth, and the bubbles rise closer to the centre than to the wall of the beds, as shown in Figs. 3 and 4. This similarity in behaviour of the particles is due to the same material properties and the same range of particle sizes contained in the different beds, although with different distributions. The flow behaviour of limestone particles is, however, a bit different. Fig. 8 shows that the transitions from one regime to another in the bed of limestone particles are sharp. This can be seen at the onset of fluidization (solids fraction fluctuations suddenly increase above 0) and prior to the onset of slugging

where the $(\sigma_{upper} - \sigma_{lower})$ curve has a pointed peak. Fig. 5 shows that bubbles rise closer to the wall than to the centre.

4.1. Minimum fluidization velocities and fluidization index

The observed minimum fluidization velocities obtained from analysis of the ECT image data are compared with those computed using the drag models given in Eq. (2) and Eq. (4). The particle shape factors used in these computations, i.e. the sphericity (φ_s) values given in Table 1, were derived by fitting Eq. (3) to the experimental data in Fig. 2 for limestone and for the 261 μm glass particles. Since the 188 μm glass particles contain the same range of particles sizes as the 261 μm glass particles, both mixtures are assumed to have the same average particle shape factor.

Fig. 10 compares the experimental minimum fluidization velocities with the computed values. The minimum fluidization velocity is plotted against the particle Archimedes number, expressed as $Ar = \frac{d_s^3 \rho_g (\rho_s - \rho_g) g}{\mu_g^2}$, which compares the net weight of a particle with the internal viscous force due to fluid flow. The result shows that the minimum fluidization velocity increases with the Archimedes number. The upper plot in Fig. 10 shows U_{mf} computed based on the estimated bed void fraction at minimum fluidization conditions using Eqs. (7) and (8). The results show that the inaccuracy in computing the minimum fluidization velocity from both drag models increases as the Archimedes number increases, although the drag model based on Gilbiaro et al. in general gives a better result and is quite close to the experimental data when $Ar < 1500$. Comparing with the computations using the void fraction obtained in the experiments (as given in Table 1), the lower plot shows that the Gidaspow model gives a better estimation. Fig. 10 shows that the computed U_{mf} are lower than the experimental values with the use of estimated ε_{mf} and higher with the use of experimental values of ε_{mf}. This shows that the value of ε_{mf} that will give a better estimation lies between the estimated and the experimental values. More so, as U_{mf} depends on the effective diameter of the particles, which depends on the particle shape, adjustment of the values of φ_s may improve the estimation.

Variations of the excess velocity to the onset of bubbling, $U_{mb} - U_{mf}$ and that of the fluidization index $\frac{U_{mb}}{U_{mf}}$ with the Archi-
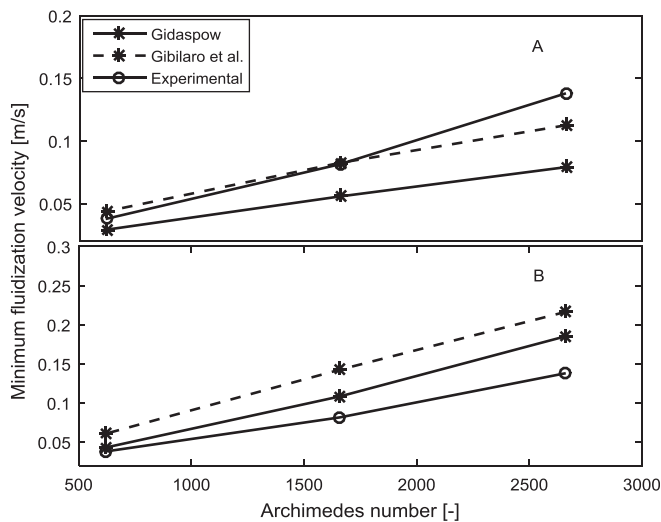
medes numbers are shown in Fig. 11. From the results, it can be seen that the excess velocity to the onset of bubbling is invariant with the particle size. This explains that most resistance to gas flow is encountered before the minimum fluidization condition, which solely depends on the particle size and density. Once bubbles begin to rise, the particle properties have less influence on the overall behaviour of the bed. The fluidization index, which decreases towards a unity as the Archimedes number increases, measures the degree to which a bed can be expanded uniformly before bubbling. This shows that with an increase in the particles size, the bed may begin to bubble without actually being expanded beyond the height at the minimum fluidization.

4.2. Superficial gas velocities at onset of slugging

As described above, the gas velocity at the onset of slugging is obtained at a point where the curve of the rate of increase in the solids fraction fluctuation at the upper plane intersects with that at the lower plane, which may occur at the peak or immediately after the peak of the $(\sigma_{upper} - \sigma_{lower})$ curve. Fig. 12 compares the experimental data with those computed from Eq. (11) at different initial bed heights. The bed height at minimum fluidization conditions used in the computation is obtained from the mass balance, which yields $h_{mf} = \frac{\varepsilon_{s0} h_0}{1 - \varepsilon_{mf}}$. The standard error bars shown in Fig. 12 indicate that the error in determining the onset of slugging by analysing the average of the five measurements (solids fraction) taken at each gas velocity is small. For the three different particles at the three different bed heights, Fig. 12 shows that the experimental data are in good agreement with the computed values. Both results show that the minimum slugging velocity increases with an increase in the particle size. Eq. (11) suggests that U_{ms} decreases with the bed height up to $h_{mf} = 60 D_b^{0.175}$, after which it increases. The value of $60 D_b^{0.175}$ defines the bed height at minimum fluidization conditions for a stable slug flow. As the computed U_{ms} for each particle decreases with the bed height, it follows that the three bed heights are below the height $60 D_b^{0.175}$ (= 90.4 cm) for a stable slug.

Fig. 12 also shows that the variations of computed U_{ms} with h_0 are almost linear, and the lines for the different particles are parallel. However, the experimental results show some degree of scatter which increases with increase in the particle size. This shows that the dependency of minimum slugging velocity on the initial bed height decreases when the particle size increases.
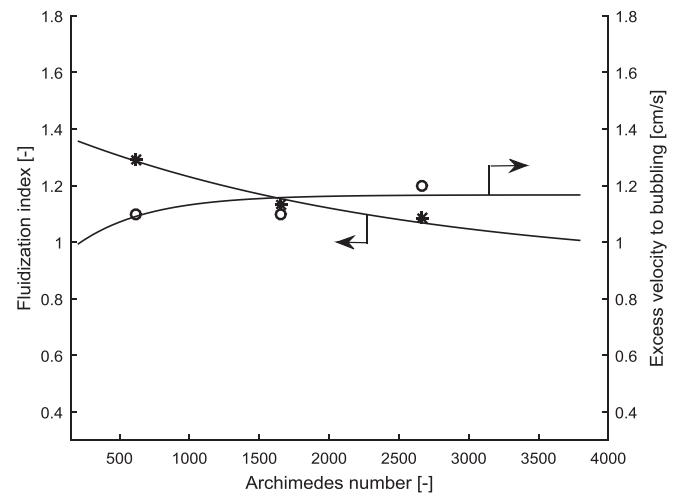

Fig. 10. Minimum fluidization velocity as a function of Archimedes number, comparing the experimental data with the computed values based on two different drag models (Gidaspow and Gilbiaro et al.), applying the estimated void fraction (upper plot, A) and the measured void fraction (lower plot, B) at minimum fluidization conditions.

Fig. 11. Influence of particle size on the onset of bubbling, showing excess velocity, $U_{mb} - U_{mf}$ and fluidization index, $\frac{U_{mb}}{U_{mf}}$ as functions of particle Archimedes number. Lines are the data fittings.
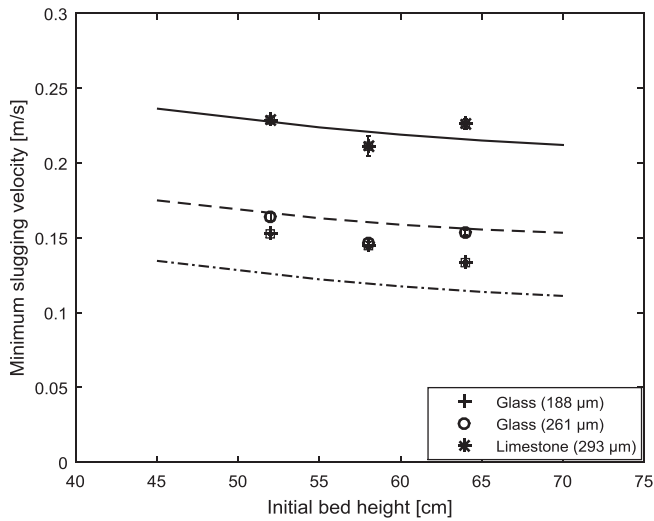
Fig. 12. Minimum superficial gas velocity for slugging as a function of bed height. Lines are the computed values from Eq. (11).
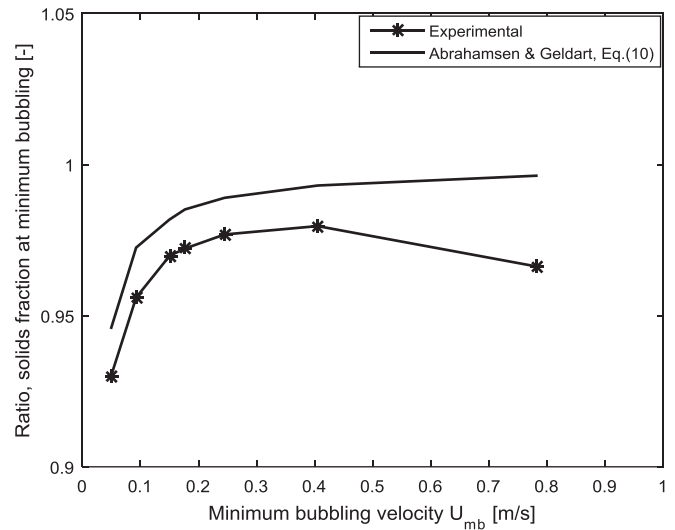

Fig. 14. Bed average solids fraction, $\frac{1-\varepsilon_{mb}}{1-\varepsilon_{mf}}$ at minimum bubbling condition as a function of minimum bubbling velocity, comparing the computed values with the experimental data.
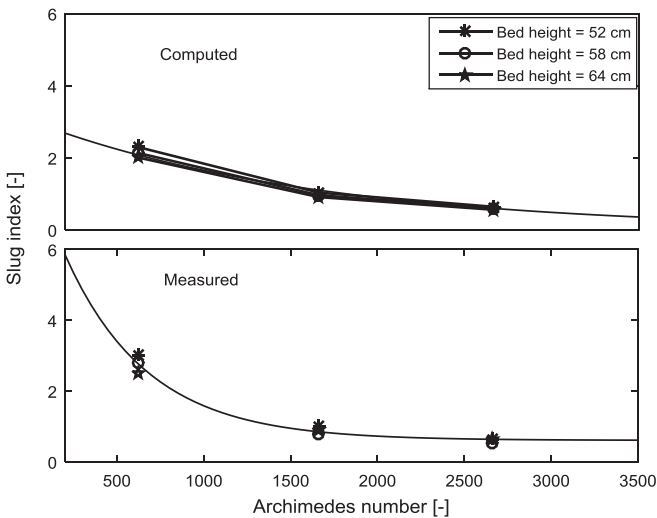

Fig. 13. Slug index, $\frac{U_{ms}-U_{mf}}{U_{mf}}$ as a function of Archimedes number, comparing the computed values (top plot) with the experimental data (bottom plot) at different bed heights. Lines are the data fittings.

The ease of bed slugging can be evaluated from the ratio $\frac{U_{ms}-U_{mf}}{U_{mf}}$, referred to as the slug index. A lower value of the slug index indicates that the bed can easily slug. Fig. 13 compares the computed slug index values with the experimental values at different Archimedes numbers. Both plots show that $\frac{U_{ms}-U_{mf}}{U_{mf}}$ decreases rapidly in the lower range of Ar and decreases slightly in the upper range.

The decrease in the value of the slug index with the Archimedes number shows that a bed of larger particles has a greater tendency to slug than a bed of smaller particles. It can also be seen that the slug index slightly depends on the bed height, and its dependency on the bed height decreases with an increasing Archimedes number. The curve fitting the experimental data suggests that the slug index approaches a stable value (in this case about 0.61) when Ar is very large, whereas the fitting of the computed $\frac{U_{ms}-U_{mf}}{U_{mf}}$ values shows that the stable slug index value is about 0.0016.

4.3. Average bed void fraction at onset of bubbling and slugging

At a given gas velocity, the average void fraction, $\varepsilon = 1 - \frac{1}{2}(\varepsilon_{s1} + \varepsilon_{s2})$ is computed for all the particles. The range of particles and bed properties considered in this study are given in Table 2.

Fig. 14 shows the variation of the measured void fraction with the minimum bubbling velocity, U_{mb}. The results show that the measured average solids fraction ratios $\frac{1-\varepsilon_{mb}}{1-\varepsilon_{mf}}$ are in good agreement with the computed values from Eq. (10). As can be seen, the solids fraction ratio increases rapidly at the lower values of U_{mb} and then slightly tends towards a constant value at the higher values of U_{mb}.

Fig. 15 shows how the bed average solids fraction $\frac{1-\varepsilon_{ms}}{1-\varepsilon_{mf}}$ at the onset of slugging varies with the slugging velocity $\frac{U_{ms}}{U_{mf}}$. Since the slug velocity ratio $\frac{U_{ms}}{U_{mf}}$ increases with a decrease in particle size, the result shows that $\frac{1-\varepsilon_{ms}}{1-\varepsilon_{mf}}$ decreases as the particle size increases. The lower value of $\frac{1-\varepsilon_{ms}}{1-\varepsilon_{mf}}$ indicates a relatively higher void at the

Table 2
Properties of fluidized beds at different regimes.

| Materials	Mean size [μm]	Density [kg/m³]	ε_{mf} [-]	ε_{mb} [-]	ε_{ms} [-]	U_{mf} [cm/s]	U_{mb} [cm/s]	U_{ms} [cm/s]
Glass	188	2500	0.430	0.450	0.526	3.80	4.90	14.50
Glass	261	2500	0.450	0.474	0.536	8.15	9.25	14.69
Limestone	293	2837	0.530	0.544	0.620	13.80	15.0	21.16
Sand	483	2650	0.460	0.475	0.565	16.50	17.66	25.82
Glass	624	2500	0.488	0.493	0.570	23.20	24.50	33.80
Limestone	697	2837	0.607	0.616	0.683	39.24	40.50	48.22
Molecular sieve	2170	1300	0.472	0.490	0.607	76.85	78.15	91.57
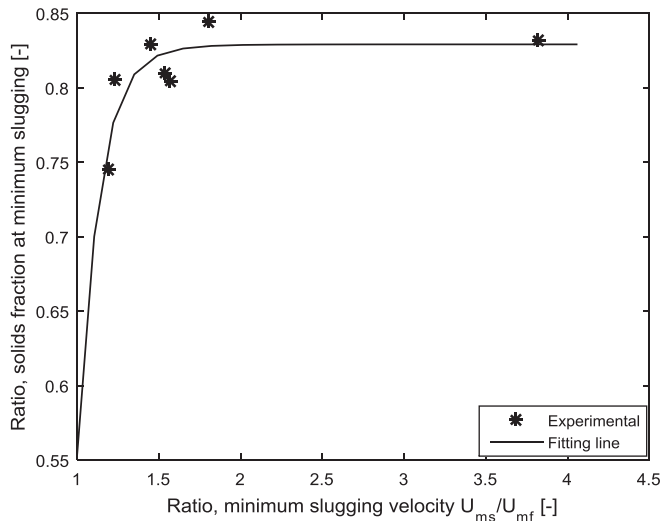
Fig. 15. Bed average solids fraction, $\frac{1-\varepsilon_{ms}}{1-\varepsilon_{mf}}$ at minimum slugging condition as a function of minimum slugging velocity ratio $\frac{U_{ms}}{U_{mf}}$.

onset of slugging compared with that at the minimum fluidization condition. The associated smaller values with larger particles follow the fact that bubbles grow faster and larger in the bed of larger particles. At the onset of slugging, bubble could even be as large as the bed diameter, leading to large void in the bed.

As can be seen, the experimental data can be fitted to a curve over the range of particle size and density considered. The curve fitting the measured solids fraction ratio at the minimum slugging condition is given in Eq. (13). This equation can be used to predict the average value of bed void fraction ε_{ms} at the minimum slugging condition.

$$\frac{1-\varepsilon_{ms}}{1-\varepsilon_{mf}} = \left[1.206 + 0.604 \left(\frac{U_{ms}}{U_{mf}} \right)^{-10} \right]^{-1} \tag{13}$$

5. Conclusions

In this study, a method is developed for determining the onsets of bubbling and slugging in a fluidized bed using a dual-plane electrical capacitance tomography (ECT) sensor. The method involves analysis of the bed behaviour at different superficial gas velocities based on the standard deviation of the solids fraction fluctuation in each plane of the sensor.

The minimum fluidization velocity is obtained where the solids fraction fluctuation begins to increase from zero. The onset of bubbling is determined when a significant bubble is first observed at the upper plane of the bed. The onset of slugging is characterized by the peak of the difference in the solids fraction fluctuation between the upper and lower planes, and is determined at the point closest to the peak where the rates of increase in the solids fraction fluctuations are the same in both planes.

The accuracy of the computed minimum fluidization velocity based on the Gidaspow [27] and the Gilbilaro et al. [29] drag models depends on the values of the particle shape factor and the bed void fraction at minimum fluidization conditions. The required value of the void fraction for accurate results was then found to lie between the measured value and the estimated value based on the Wen and Yu empirical expressions. With an increase in the particle size, the fluidization index decreases while the excess velocity to the onset of bubbling appears relatively the same. Both the particle size and the bed height influence the transition from bubbling to slugging. The larger the particle size is, the greater is

the particle tendency to slug. The dependency of minimum slugging velocity on the bed height decreases with increase in the particle size. The ratio of the average solids fraction at the onset of slugging to that at onset of fluidization appears to be constant for small particles, but decreases with an increase in the particle size for larger particles. Based on the experimental data obtained over a wide range of particle size 180–2200 μm, a correlation was developed for prediction of average bed void fraction at the onset of slugging.

Furthermore, the three different particle samples primarily considered in this study show that the method developed in this paper for determining the onset of slugging in a fluidized bed is consistent with different material properties (sphericity, density and size distributions). Fitting of the experimental data suggests that a set of empirical correlations as a function of the Archimedes number can be obtained for estimating the velocities at the onset of fluidization (minimum fluidization velocity), at the onset of bubbling and at the onset of slugging, but this will require more experimental data in a future work.

Funding sources

Appendix A. Supplementary data

Supplementary data associated with this article can be found, in the online version, at http://dx.doi.org/10.1016/j.cej.2017.07.098.

References

[1] C. Alberto, S. Felipe, S.C.S. Rocha, Time series analysis of pressure fluctuation in gas-solid fluidized beds, Braz. J. Chem. Eng. 21 (2004) 497–507.
[2] B. Du, W. Warsito, L.-S. Fan, ECT studies of gas-solid fluidized beds of different diameters, Ind. Eng. Chem. Res. 44 (2005) 5020–5030.
[3] R.K. Padhi, Y.K. Mohanty, G.K. Roy, B. Sarangi, Hydrodynamic studies of gas solid fluidization in non- cylindrical conduits for spherical and non-spherical particles – a review, Int. J. Sci. Res. Publ. 3 (2014) 1–8.
[4] D. Kunii, O. Levenspiel, Fluidization Engineering, second ed., Butterworth – Heinemann, Washington Street, USA, 1991.
[5] X. Bi, Flow Regime Transitions in Gas-Solid Fluidization and Transport, PhD thesis, Department of Chemical Engineering, the University of British Columbia, 1994.
[6] P.W.K. Kehoe, J.F. Davidson, Continuously slugging fluidized beds, chemeca '70, Inst. Chem. Eng. Symp. Ser. 33 (1970) 97–116.
[7] J. Baeyens, D. Geldart, An investigation into slugging fluidized beds, Chem. Eng. Sci. 29 (1974) 255–265.
[8] R. Cliff, J.R. Grace, M.E. Weber, Bubbles, Drops and Particles, Academic Press, New York, 1978.
[9] J.T. William, E.P. Owen, Slugging in fluidized beds, Ind. Eng. Chem., Fundam. 16 (1977) 242–247.
[10] R. Roy, J.F. Davidson, V.G. Tuponogov, The velocity of sound in fluidized beds, Chem. Eng. Sci. 45 (1990) 3233–3245.
[11] J.R. Grace, Agricola aground: characterization and interpretation of fluidization phenomena, AIChE Symp. Ser. 88 (1992) 1–16.
[12] C. Rautenbach, R.F. Mudde, X. Yang, M.C. Melaaen, B.M. Halvorsen, A comparative study between electrical capacitance tomography and time-resolved X-ray tomography, Flow Measur. Instrum. 30 (2013) 34–44.
[13] M. Puncochar, J. Drahos, J. Cermak, K. Selucky, Evaluation of minimum fluidization velocity in gas fluidized bed from pressure fluctuations, Chem. Eng. Commun. 35 (1985) 81–87.
[14] C.A.S. Felipe, S.C.S. Rocha, Prediction of minimum fluidization velocity of gas-solids fluidized beds by pressure fluctuation measurements – analysis of standard deviation methodology, Powder Technol. 174 (2007) 104–113.
[15] D. Wilkinson, Determination of minimum fluidization velocity by pressure fluctuation measurement, Can. J. Chem. Eng. 73 (1995) 562–565.
[16] C. Rautenbach, M.C. Melaaen, B.M. Halvorsen, Possible identification of size difference segregation using electrical capacitance tomography and statistical analysis, Eur. J. Sci. Res. 11 (2013) 351–364.
[17] Y.T. Makkawi, P.C. Wright, Fluidization regimes in a conventional fluidized bed characterized by means of electrical capacitance tomography, Chem. Eng. Sci. 57 (2002) 2411–2437.
[18] W. Kong, T. Tan, J. Baeyens, G. Flamant, H. Zhang, Bubbling and slugging of geldart group a powders in small diameter columns, Ind. Eng. Chem. Res. 56 (2017) 4136–4144.

[19] L.-P. Leu, F.-C. Tsai, Hydrodynamics of Geldart group A particles in gas-solid fluidized beds, Kor. J. Chem. Eng. 26 (2009) 513–517.
[20] D.G. Dimattia, P.R. Amyotte, F. Hamdullahpur, Slugging characteristics of group d particles in fluidized beds, Can. J. Chem. Eng. 75 (1997) 452–459.
[21] T.E. Broadhurst, H.A. Becker, Onset of fluidization and slugging in beds of uniform particles, AIChE J. 21 (1975) 238–247.
[22] T.C. Ho, N. Yutani, L.T. Fan, W.P. Walawender, The onset of slugging in gas fluidized beds with large particles, Powder Technol. 35 (1983) 249–257.
[23] I. Noordergraaf, W.A. Van Dijk, C.M. Van Den Bleek, Fluidization and slugging in large-particle systems, Powder Technol. 52 (1987) 59–68.
[24] F. Taghipour, N. Ellis, C. Wong, Experimental and computational study of gas-solid fluidized bed hydrodynamics, Chem. Eng. Sci. 60 (2005) 6857–6867.
[25] S. Benzarti, H. Mhiri, H. Bournot, Drag models for simulation gas-solid flow in the bubbling fluidized bed of FCC particles, Int. J. Chem. Mol., Nucl., Mater. Metall. Eng. 6 (2012) 111–116.
[26] P. Li, X. Lan, C. Xu, G. Wang, C. Lu, J. Gao, Drag models for simulating gas-solid flow in the turbulent fluidization of FCC particles, Particuology 7 (2009) 269–277.
[27] D. Gidaspow, Multiphase Flow and Fluidization: Continuum and Kinetics Theory Descriptions, Academic Press Inc., San Diego, California, USA, 1994.
[28] S. Ergun, Fluid flow through packed column, Chem. Eng. Progr. 48 (1952) 89–94.
[29] L.G. Gibilaro, R. Di – Felice, S.P. Waldram, Generalized friction factor and drag coefficient for fluid-particle interaction, Chem. Eng. Sci. 40 (1985) 1817–1823.
[30] C.Y. Wen, Y.H. Yu, A generalized method for predicting the minimum fluidization velocity, AIChE J. 12 (1966) 610–612.
[31] D. Geldart, Types of gas fluidization, Powder Technol. 7 (1973) 185–195.
[32] D. Geldart, A.R. Abrahamsen, Homogeneous fluidization of fine powders using various gases and pressures, Powder Technol. 19 (1978) 133–136.
[33] H.I. de Lasa (Ed.), Chemical Reactor Design and Technology:- Overview of New Development of Energy and Petroleum Reactor Technologies Projection for the 90's, Martinus Nijhoff Publishers, 1986.
[34] W.C. Yang (Ed.), Handbook of Fluidization and Fluid-Particle Systems, Marcel Dekker, Inc., 2003.
[35] D. Geldart, Chapter 4, Gas Fluidization Technology, first ed., John Wiley & Sons, Ltd., 1986, pp. 53–97.
[36] Process Tomography, Electrical Capacitance Tomography System. Operating Manual Volume 1: Fundamentals of ECT, Process Tomography Ltd., 2009.
[37] R.K. Thapa, B.M. Halvorsen, Study of Flow Behaviour in Bubbling Fluidized Bed Biomass Gasification Reactor using CFD Simulation. in: Proceedings of the 14th International Conference on Fluidization – from Fundamentals to Products, Eds. ECI Symposium Series, Volume, 2013.